



HAL
open science

Strain localization and anisotropic correlations in a mesoscopic model of amorphous plasticity

Mehdi Talamali, Viljo Petäjä, Damien Vandembroucq, Stéphane Roux

► **To cite this version:**

Mehdi Talamali, Viljo Petäjä, Damien Vandembroucq, Stéphane Roux. Strain localization and anisotropic correlations in a mesoscopic model of amorphous plasticity. 2011. hal-00483291v2

HAL Id: hal-00483291

<https://hal.science/hal-00483291v2>

Preprint submitted on 17 Jan 2011 (v2), last revised 13 Feb 2012 (v4)

HAL is a multi-disciplinary open access archive for the deposit and dissemination of scientific research documents, whether they are published or not. The documents may come from teaching and research institutions in France or abroad, or from public or private research centers.

L'archive ouverte pluridisciplinaire **HAL**, est destinée au dépôt et à la diffusion de documents scientifiques de niveau recherche, publiés ou non, émanant des établissements d'enseignement et de recherche français ou étrangers, des laboratoires publics ou privés.

Strain localization and anisotropic correlations in a mesoscopic model of amorphous plasticity

Mehdi Talamali,¹ Viljo Petäjä,² Damien Vandembroucq,¹ and Stéphane Roux³

¹ *Laboratoire PMMH, CNRS/ESPCI/UPMC/Univ. Paris 7 Diderot
10 rue Vauquelin, 75231 Paris cedex 05, France*

² *Laboratoire SVI, Unité Mixte CNRS/Saint-Gobain*

39 quai Lucien Lefranc, 93303 Aubervilliers cedex, France

³ *LMT-Cachan, ENS de Cachan/CNRS-UMR 8535/UPMC/PRES UniverSud Paris
61 Avenue du Président Wilson, 94235 Cachan cedex, France*

A mesoscopic model for shear plasticity of amorphous materials in two dimensions is introduced, and studied through numerical simulations in order to elucidate the macroscopic (large scale) mechanical behavior. Plastic deformation is assumed to occur through a series of local reorganizations. Using a discretization of the mechanical fields on a discrete lattice, local reorganizations are modeled as local slip events. Local yield stresses are randomly distributed in space and invariant in time. Each plastic slip event induces a long-ranged elastic stress redistribution. Rate and thermal effects are not discussed in the present study. Extremal dynamics allows for recovering many of the complex features of amorphous plasticity observed experimentally and in numerical atomistic simulations in the quasi-static regime. In particular, a quantitative picture of localization, and of the anisotropic strain correlation both in the initial transient regime, and in the steady state are provided. In addition, the preparation of the amorphous sample is shown to have a crucial effect of on the localization behavior.

I. INTRODUCTION

The prominent mechanical property of glasses is their brittleness. Nevertheless, the question of their possible plasticity has been discussed very early [1, 2]. Limited to small scale or confined geometries (due to their brittleness), the plastic behavior of glasses is quite different from its crystalline counterpart. In particular, a notable pressure-dependence is often encountered and, in addition to shear flow, it is common to observe permanent densification [3–7]. Despite this early interest for the plastic behavior of oxide glasses and the primary importance of this phenomenon for mechanical contact properties, the subject has long remained poorly explored.

Several obstacles which have for long limited the study of amorphous plasticity have been progressively lifted in the recent years. The use of local techniques such as atomic force microscopy [8] or micro-spectroscopy [9] has for instance given access to additional experimental data allowing one to test plastic criteria at macroscopic scales [10]. The recent development of metallic glasses has given a new momentum to this subject [11]. Indeed, the mechanical strength of metallic glasses appears to be limited by shear-banding induced failure phenomena.

One of the most important issues that constitute a barrier in the development of those materials is the proper mastering of size effects. Indeed, if the yield limit appears to be extremely high as compared to crystalline materials with the same chemical composition, yet failure appears to be quite brutal for large scale specimens, akin to brittle fracture. Amazingly, a closer analysis show that these materials may withstand a large number of macroscopic slips over different shear planes prior to failure (see Fig. 1) [12]. At a large scale, macroscopic phenomena such as thermal softening induced by plastic dissipation are essential in order to address such macroscopic observations. However, the initiation of localization is believed to occur at a much smaller scale where heat dissipation is presumably ineffective. The proper understanding of the initiation of inhomogeneous plastic strain is thus essential to enhance the mechanical properties of these materials.

It is also essential when designing simulation methods which are not attached to a specific scale (such as Molecular Dynamics). The fast development of computing facilities has opened the way to direct simulations of shear plasticity of glasses [13–37] using atomistic simulations, at nanometer scales. Finally, a major theoretical difficulty lied in the absence for amorphous materials of any obvious microscopic alternative concept to dislocations for crystalline plasticity. The understanding that plastic deformation resulted from a series of local structural reorganizations [13, 38], commonly referred to as “shear transformation”, (ST), was a major theoretical breakthrough.

A. Molecular Dynamics

In view of the obvious numerical limitations of atomistic simulations, most of the recently simulated systems consisted of 2D Lennard-Jones model glasses or close variants [13, 15, 18, 20–22, 26, 27, 29, 30, 32–35, 39–41] which

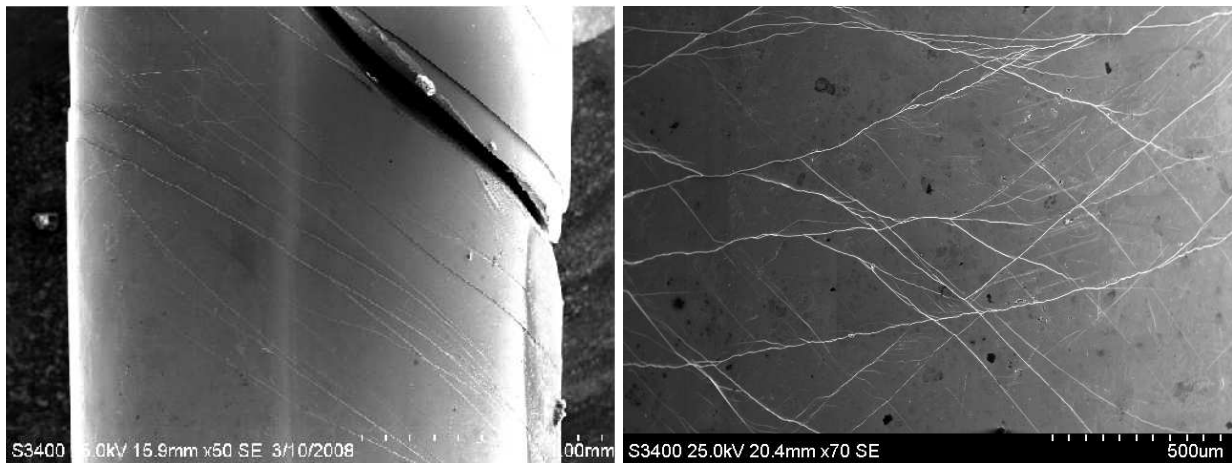


FIG. 1: Post-mortem Scanning Electronic Microscopy images of the side view of a cylindrical shaped bulk metallic glass specimen subjected to an axial compression. The left view shows a dense distribution of straight shear bands parallel to the final failure surface. The right one is a closer view of the cylinder side where the slip direction is mostly anti-plane. (Courtesy of J. Zhang and P. Aimeidieu[12])

already capture most of the difficulties of the problem, and yet allowed to consider large system sizes. A few three dimensional works [23, 28] indeed confirmed that little new physics emerged from the third dimension. Some simulations even made use of more “realistic” potentials for metallic glasses [17], amorphous silicon, [19, 24, 25, 36], vitreous polymers [14, 16] or silica glass [31, 37] reaching similar conclusions. Note that in the case of silica glass, in addition to the studies under shear a large number of studies have been dedicated to the phenomenon of permanent densification under high hydrostatic pressure [42–50].

Beyond the question of the microscopic mechanisms, a special attention has been devoted to the complex character of the plastic behavior of glasses. At a microscopic scale, the “non-affine” corrections to the elastic behavior have been thoroughly discussed [15, 20–22, 27, 29, 31, 34, 35, 51] as well as their possible consequences on the initiation of plastic reorganizations [35]. Strain localization has received a particular interest [18, 26, 28, 39, 52] as well as avalanche statistics [20, 40]; akin to other non-linear mechanical behaviors in random media (e.g. fracture), plastic deformation is not continuous but proceeds by successive bursts.

B. Meso-models

In parallel to the above discussed atomistic simulations, several works have developed numerical models at a mesoscopic scale, *i.e.* intermediate between the scale of an individual reorganization and the macroscopic scale where continuum mechanics gives a faithful description. Assuming that plastic deformation resulted from a series of reorganizations, Argon and Bulatov early proposed a discrete model of amorphous plasticity and studied its behavior at different temperatures [53–55]. Homer and Schuh [56] very recently proposed an extension of this model to follow the dynamics of plastic deformation of amorphous metals under shear using a kinetic Monte-Carlo algorithm.

Along similar ideas, Baret *et al.* [57] developed a model of amorphous plasticity at zero temperature in antiplane geometry with two main ingredients: a structural disorder and a long-range elastic interaction to account for the stress redistribution due to local plastic reorganizations. This model, which exhibits critical properties, can also be considered as belonging to the same vein as other statistical modeling for earthquakes [58, 59] or elastic line depinning [60, 61]. In a close spirit, Picard *et al.* discussed complex spatio-temporal behavior of a yield stress fluid [62]. In this model, the authors considered a quadrupolar elastic interaction but no other source of disorder than the one caused by the relaxation dynamics. Following similar ideas, Bocquet *et al.* developed an analytic model for the elastoplastic dynamics of a jammed material taking into account the elastic stress redistribution[63]. Lemaître and Caroli[64] recently discussed the avalanche behavior within a mean field model. In particular, they proposed to link ideas of effective temperature discussed by Sollich *et al.* [65] to describe the rheology of soft glasses and the internal stress fluctuations by varying the distribution of their elastic interaction. Jagla [66] discussed the effect of a local relaxation processes on the localization behavior. Sekimoto[67] discussed the internal stress as encoding past mechanical treatments. In a more traditional dislocation plasticity spirit, Zaiser and Moretti[68] discussed the avalanche behavior in a mesoscopic model very close to the above discussed ones. More recently Dahmen *et al.*[69]

proposed a variant of the mean field Ben-Zion–Rice earthquake model[59] incorporating a systematic weakening or hardening effect.

C. Macroscopic scale

Some of these studies have been dedicated to the characterization of the plastic behavior within a continuum mechanics framework [14, 16, 17]. Although a wide consensus exists on the scenario of STZ proposed by Falk and Langer [13] as validated by the numerous numerical studies [15, 19–21, 24, 25, 29, 34–36, 70, 71], the quantitative characterization of these local reorganizations as well as their links to the local structure remains quite elusive. The large scale behavior is observed to approach a so-called elastic-perfectly plastic constitutive law, where the macroscopic stress becomes independent from the macroscopic strain. However, the latter law lies at the edge of mechanical stability. Would stress increases with strain (“hardening” behavior) that the macroscopic strain field would tend to be homogeneous at large scales (under a uniform stress). In contrast, a “softening” behavior (where stress decreases with strain) induces at large scales localization modes where strain concentrates on shear bands. In the latter case, homogenization is inappropriate. The perfectly plastic behavior lies at the borderline between these two classes of behavior. Hence, one cannot state any general results about the homogeneity of the strain field. Hence it is necessary to resort to microscopic details, as they will determine the answer to such a question. The vanishing of the tangent stiffness is thus the key feature that allows for the relevance of more microscopic details than in hardening behaviors. However, not all details matter, and sorting out the important ingredients needed to enrich an effective macroscopic description is an important issue which has not been addressed as such in the abundant above mentioned literature. In conclusion, a clear view of up-scaling is still missing. This question is limiting inasmuch as the identification of a proper continuum description framework is not settled (*e.g.* is the plastic strain field uniformly distributed or rather localized in the thermodynamic limit?) and hence the question of what microscopic features survive at a macroscopic scale and should be extracted from extensive microscopic studies is not elucidated yet. The present work aims at addressing the question of the asymptotic homogeneity or heterogeneity of the plastic strain over various space and time scales. In order to approach this problem, we will consider a large scale modeling and argue for the relevance at large scales of the elementary mechanisms in line with microscopic or mesoscopic modeling. This model will be seen to reproduce the early work by Baret *et al* [57] in the context of anti-plane loading. The latter case corresponds to a parallel displacement field along say the z -axis, whose amplitude depends only on the transverse coordinates $U_z(x, y)$. We will rather focus here on a different symmetry, *e.g.* plane strain, where $U_z = 0$, and the in-plane displacement depends only on x and y . Because the modeling is proposed based on large scale asymptotics, we will retain only the most salient effects which have a chance to survive at a large scale and hence, our objective is to propose the minimal level of complexity. Nevertheless, a detailed comparison of scaling features with microscopic modeling such as that of Maloney and Robbins[39] can be performed and will be shown to be extremely close.

In this paper, a particular emphasis is put on the geometrical features of the plastic strain field. The model is constructed in Section II, the stress-strain relation is discussed in Section III, the localization behavior is discussed in Section IV. Section V gives a quantitative characterization of the anisotropic strain correlation. A final discussion, Section VII, concludes this article.

II. DEFINITION OF THE MODEL

The studied model is here constructed with the objective of capturing the *large scale behavior* of amorphous media. In order to limit the computational cost of studying the model, only the two dimensional case of plane strain will be considered. It is recalled that similar behaviors were observed in molecular dynamics simulations in two and three dimensions, and hence this restriction is not limiting. As argued in the introduction, the macroscopic loading may induce changes in volume which are coupled with the activation of plastic flow. However, for extended shear, no macroscopic dilation or shrinkage is expected and hence the dominant macroscopic plastic strain will be deviatoric. Hence for simplicity pure shear boundary conditions are considered, with fixed principal axes in order to reach large strains. More precisely the mean total strain field is controlled as

$$\langle \varepsilon \rangle = \varepsilon \begin{pmatrix} 1 & 0 \\ 0 & -1 \end{pmatrix} \quad (1)$$

In the following a discretization will have to be introduced to study numerically the model. A square lattice with bi-periodic boundary conditions will be used to avoid a systematic spatial bias induced by rigid boundaries.

The microscopic structure of amorphous media is intrinsically heterogeneous, and hence, in the absence of plastic reorganization, the elastic behavior of the material is heterogeneous. However, upon coarse-graining, this heterogeneity will vanish giving rise to an homogeneous behavior for which elastic constants can be derived from classical homogenization techniques. Thus, the elastic regime will be described as homogeneous. Moreover, the amorphous medium will be assumed to be isotropic. Although this has been questioned on the basis of molecular dynamics simulation for amorphous silica [37], such an anisotropy is weak and does not affect the main features (and in particular scaling properties) of the model at large scales. Since no volume change will be considered, only one elastic constant, the shear modulus, μ , has to be introduced, which is considered in the following to be $2\mu = 1$.

The shear transformations are the only source of non-linearity in the model, and hence at any stage, the medium can be unloaded and reloaded by the mere superposition of a uniform shear stress field (with a fixed orientation). Hence, the tensor stress field can be characterized by its sole deviatoric norm (or equivalent von Mises stress). Scalar (equivalent) stress $\sigma \equiv \sigma_{xx} - \sigma_{yy}$ and strain $\varepsilon \equiv \varepsilon_{xx} - \varepsilon_{yy}$ will be used (although we use a plane strain assumption, the conditions specified below will guaranty that plane stress also hold). The latter scalar stress component will be denoted as σ , and called “stress” for simplicity. Similarly a single scalar strain component will matter, and will be denoted as the strain, ε , in the sequel. With those notations the incremental elastic law reduces to the elementary form $\Delta\sigma = \Delta\varepsilon$.

As above discussed, in amorphous materials such as glasses, pastes or foams, a common assumption consists in describing the macroscopic deformation as deriving from a succession of localized reorganizations at some microscopic scale [13]. These regions can be seen as the coarse grained Shear Transition Zones (STZ) [13] whose sizes reach at most a few tens of atoms [30] in molecular dynamics simulations. The details of such local rearrangements depend obviously on the precise structure of the material under study. They involve local change in the topology of atoms, grains or foam cells, and significant non-linearities either of geometrical or constitutive origin take place. The important feature is that these reorganizations are local in space. We discuss below the criterion to initiate such an event (Sect. II A) and its effect on the stress field (Sect. II B).

A. Onset of local plastic transformation

In order to describe at which stage of loading such a shear transformation will take place, a criterion has to be proposed. It is natural in the present framework to characterize locally the onset of a transformation through the local stress. We recall that here local refers to our discretization which is itself a mesoscopic scale not to be confused with the microscopic one. Let us only note here that the full characterization of the local reorganization occurring under shear in amorphous materials is still a ongoing issue. In particular the existence for amorphous materials of a local stress threshold at atomic scale has recently been debated [34, 72]. While the definition of a satisfactory criterion can be discussed at atomic scale, there is no doubt however that under sufficient coarse graining, one should recover a criterion based upon the stress tensor. Irrespectively of the precise characterization of local instabilities at atomic scale, we assume in the present mesoscale model, that the coarse-graining is performed at a large enough length scale to allow us to safely use local yield stress criteria. The criterion for yielding characterizes the local configuration of atoms, and hence will display some variability. A local yield threshold for each discrete site \mathbf{x} as $\sigma_\gamma(\mathbf{x})$ is introduced, and will be treated as a random variable in the sequel. For all sites, the same statistical distribution will be used, chosen for simplicity as a uniform distribution over the interval $[0, 1]$. Other distributions could be considered but are not expected to alter the generic behavior of the model beyond a few mesh sizes.

It is to be noted that since no stress scale has been introduced in the model so far, rescaling the distribution to $[0, \varsigma_1]$ will only multiply all stresses by the same factor ς_1 . Similarly, the interval may be translated to $[\varsigma_0, \varsigma_0 + \varsigma_1]$, by adding a constant ς_0 to all stresses. Thus the linearity of the model can be exploited to match any yield stress interval. More importantly, other distributions, such as a Gaussian, behave similarly, and at a large enough scale, the local yield distribution can no longer be read from macroscopic observables, as a consequence of universality.

B. Effect of a local transformation

Beyond the confined region where the rearrangement takes place, a stress perturbation has to be accommodated by elastic strain throughout the material. This perturbation induces internal elastic stresses σ_{el} which vanish with the distance, as dictated by linear elasticity (of a homogeneous medium as above argued). The general solution of elastic field induced by a localized perturbation can be written easily as discrete infinite series (multipolar expansion [73]). An important feature of those modes is the absence of length scale. Therefore, these influence functions can be extrapolated down to a point-like singularity. As such, they are genuine Green functions attached to the elementary rearrangements. The constraint of not imposing externally any force or torque selects fields which decreases with the

distance to the transformation zone as r^{-n} where $n \geq d$ where d is the space dimension. The leading perturbation term is hence given only with the $n = d$ terms. Three such modes exist in two dimensions, $d = 2$, which coincide with the external problem of a plastic strain imposed uniformly in a circular inclusion, the so-called Eshelby problem. One is a pure dilation which corresponds to the expansion or shrinkage of the transformation zone. The two others are pure shear modes with different principal axes. Because the macroscopic loading is a pure shear, and large plastic strains are considered, the dilation mode will vanish on average. Hence, any change of volume will be discarded. Similarly, on average, the orientation of the deviatoric mode will be aligned with the macroscopic loading, and fluctuations around this orientation will be neglected. Hence only one mode will be retained to describe the elastic effect of a localized transformation. Mesoscopic scale models such as [57, 62] thus consist in studying the effect of these dominant terms of the elastic interaction on the dynamics of localized plastic events, independently of the microscopic details. It is stressed that there is no upper limit on the discretization scale, since the considered Eshelby mode does not involve any specific length scale. However, if the discretization scale changes, the corresponding statistical features of the local rearrangements have to be coarsened at the appropriate scale and hence the microscopic disorder has to be adjusted to match a specific material. This question will not be addressed in the present study.

An elementary local transformation zone occurring at point \mathbf{x}_0 is thus described by a stress field $\eta G(\mathbf{x} - \mathbf{x}_0)$ whose scalar amplitude η is the only relevant feature. Note that the translational invariance which is natural in an infinite medium still holds for the chosen bi-periodic boundary conditions in a finite size system. The precise form of G is discussed below in Sect. II D. Reverting to the original Eshelby problem, this amplitude can be interpreted as the product of a uniform plastic strain within a circular inclusion times its volume (or area in our two-dimensional framework). But the key point, is that the external stress field is independent of the specific shape of the inclusion and details of the re-arrangement. Nor does it make sense to distinguish separately volume and local plastic strain. In the sequel, conventionally the volume of the STZ can thus be chosen to be equal to the volume of the discretization scale, namely unity, and hence the amplitude η is a measure of the equivalent local plastic strain, denoted as “local slip” in the following.

An elementary local transformation of amplitude η occurring at point \mathbf{x}_0 induces a local increase in the plastic strain field

$$\Delta \varepsilon_p(\mathbf{x}) = \eta \delta(\mathbf{x} - \mathbf{x}_0) \quad (2)$$

where δ is the Dirac distribution. The residual stress field σ_{el} is correspondingly modified by

$$\Delta \sigma_{el}(\mathbf{x}) = \eta G(\mathbf{x} - \mathbf{x}_0) \quad (3)$$

This residual stress field itself encodes a memory of the set of transformations experienced by the medium, and long-range spatial correlation will naturally accumulate in the stress field. Thus at any stage of loading the local stress consists of a homogeneous macroscopic stress, Σ , added to the residual stress field,

$$\sigma(\mathbf{x}) = \Sigma + \sigma_{el}(\mathbf{x}) \quad (4)$$

As local transformations can occur anywhere in space, each point \mathbf{x} is attributed a threshold stress $\sigma_\gamma(\mathbf{x})$. Starting from rest, at each instant of time, we deduce the level of external loading needed to trigger a local transformation as

$$\Sigma_c = \min_{\mathbf{x}} [\sigma_\gamma(\mathbf{x}) - \sigma_{el}(\mathbf{x})] \quad (5)$$

The intrinsic local disorder of amorphous media implies that the slip amplitudes η are randomly distributed. Moreover, because our description is sought at a large scale no spatial nor temporal correlations will be considered. To account for the local reorganizations, it thus suffices to give the probability distribution function of their (scalar) amplitude. The only physical constraint is that they should be bounded. Similarly to the yield thresholds, the slip value η is drawn randomly from the uniform distribution, $[0, d]$ if not otherwise stated. d is a parameter of the model whose role will be discussed below.

C. Extremal dynamics

Quasi-static driving conditions are considered. Thus stress redistribution is considered to occur instantaneously (no viscous effect are considered). However, one should finally specify the way the system is driven. A constant external stress is inappropriate as one expects the stress strain law to tend to a constant plateau stress. An imposed total strain is more relevant, but it has the drawback of possibly triggering multiple transformation zones. We have chosen the so-called “extremal dynamics”, which consists of adjusting at each instant of time the external loading Σ

so that one and only one transformation zone $\mathbf{x}^*(t)$ is activated at each time t according to Eq. 5. This may involve a reduction in the applied macroscopic stress and strain. A unique temporal sequence of event is selected, from which it is easy to reconstruct any other driving mode assuming the same sequence of events. In this way, “avalanches” can be defined without ambiguity. Note however, that “time”, t , is used here as a simple way of counting and ordering events. On average, time is simply proportional to the total plastic strain imposed on the system, $\langle \varepsilon_p \rangle = t d L^{-2} / 2$. The plastic strain field is thus simply

$$\varepsilon_p(\mathbf{x}, t) = \sum_1^t \eta(t) \delta(\mathbf{x} - \mathbf{x}^*(t)) \quad (6)$$

It can be shown that this specific driving mode is precisely the one that would result from an over-damped viscous dynamics and infinitesimal strain rate driving.

D. Stress redistribution function

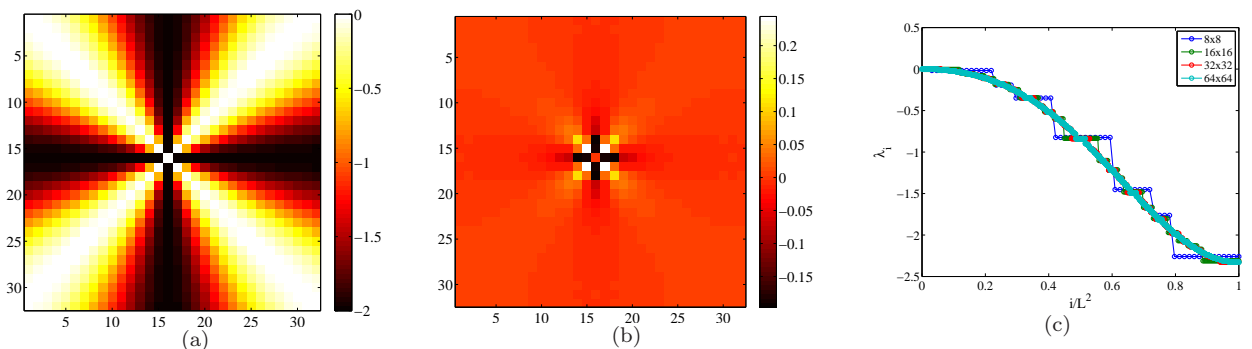


FIG. 2: Map of the quadrupolar elastic interaction used in the model. The discretization is performed in the Fourier space $\tilde{G}(k, \omega) = \cos(4\omega) - 1$, where k and ω are the polar coordinates in the Fourier space (a) and a subsequent Fourier transform gives in the direct space the Green function $G(r, \theta)$ (b) satisfying the bi-periodic boundary conditions of the problem. (c) Spectrum of the eigenvalues of the elastic propagator. The horizontal tangent at the maximum eigenvalue zero can be associated to an abundance of soft modes (with null or close to zero eigenvalues). The associated eigen-modes are aligned along directions equal or close to $\pm 45^\circ$.

The Green function G can easily be computed to be $G = \cos(4\theta)/r^2$ in polar coordinates for an infinite medium. The quadrupolar elastic kernel is obviously a key ingredient of the present model. As already discussed by Picard *et al* [62], the numerical implementation of this kernel is rather delicate. In order to deal with the bi-periodic boundary conditions we chose here to discretize first in the reciprocal space $\tilde{G}(k, \omega) = \cos(4\omega) - 1$, where k and ω are the polar coordinates in the Fourier space, (Fig. 2a) then to Fourier transform to get the periodic kernel $G(r, \theta)$ in the direct space (Fig. 2b). In the present case, because of the bi-periodic boundary conditions, the elastic propagator is a circular matrix. The eigenvalues of this (convolution) operator are directly obtained by Fourier transforming the associated Green function. At the same time as the elastic propagator we thus obtain the spectrum of its eigenvalues, as shown in Fig. 2c, without performing any further computation.

The residual stress field resulting from an arbitrary cumulative plastic strain is easily written in Fourier space as

$$\tilde{\sigma}_{el} = \tilde{G} \cdot \tilde{\varepsilon}_p \quad (7)$$

Hence integration over a long interval of time shows that a stationary state can be reached where σ_{el} remains constant, while plastic strain accumulates over the modes associated with a zero eigenvalue for G . This shows trivially that uniform shear along lines at $\pm\pi/4$ orientation with respect to the x -axis, but with arbitrary values from line to line meets this stationary condition. However, as plasticity develops in our model by discrete events of random amplitude, it is not possible to fulfill such condition at each instant of time. The “granularity” of the elementary events imposes a locality of plastic strain in real space, which in turn is non-local in Fourier space, and hence, stress fluctuations will occur for which it is essential to account faithfully for the vicinity of the spectrum of eigenvalues close to 0. This point is emphasized here because slight variations in the discretization of the Green function G which may appear as innocuous have a drastic influence in the scaling properties of the model.

E. Slip amplitude distribution

Let us come back to the meaning of the parameter d which is the only dimensionless parameter of the model. It quantifies the elementary plastic strain required to change the conformation of the local shear transformation zone, at the scale, a , of our discrete mesh in such a way that local yield stress correlation over time can be ignored. After one elementary local transformation event, the stress fluctuation for a site neighbor to the slip is of order d . This quantity is to be compared to the amplitude of the yield stress fluctuations, ς_1 . Hence the important dimensionless parameter is d/ς_1 . In the sequel, the yield stress amplitude ς_1 is conventionally set to unity. d remains the only free parameter of the model. For most of the simulations shown below, a value of $d = 0.01$ is chosen.

In the following we will focus on the relation between the local plasticity events and the macroscopic plastic flow. We will show in particular that a scale invariant picture naturally emerges (and whose justification lies in the underlying criticality of the depinning transition). It is therefore extremely important to identify those statistical features in order to be able to up-scale the description, and capture the transition toward a deterministic behavior at a large enough scale.

III. STRESS-STRAIN RELATION

The choice of an extremal dynamics corresponds to a quasistatic driving at a vanishing strain rate. While the strain rate is kept constant, the external stress is a highly fluctuating quantity. Far from being restrictive, this choice allows us to visit all successive configurations of the system and to reconstruct the response to any loading. The case of the response to a monotonically increasing stress is recovered by computing the maximum external stress over the past. However as this quantity is controlled by one single event in the past, it is a fragile quantity. In the following, the time evolution is cut into intervals corresponding to a number of event equal to the number of sites in the system (so that the mean plastic strain increment is $d/2$). The macroscopic stress is computed as the maximum external stress over each interval. Fig. 3 shows the evolution of this quantity, denoted here $\langle \Sigma \rangle$ as a function of the plastic strain for different values of the slip increment parameter d .

It is to be noted that the stress-strain curve appears here to be a well-behaved quantity which is independent of the system size in the explored range ($L = 16$ to $L = 256$ for different values of the slip increment parameter $d = 0.01, d = 0.1, d = 1$ in Figure 3). Saturation occurs at a d -dependent value of the plateau stress. However, as can be seen in Figure 3, for higher values of d , a systematic size effect can be seen. It affects only the smallest sizes for $d = 0.1$, but appears to be very significant for sizes ranging from 16 to 256 when $d = 1$.

A simple argument allowing us to rationalize the dependence of the plateau stress on the slip increment parameter d consists of regarding the elastic stress fluctuations as some kind of mechanical noise. Using this analogy early proposed by Sollich *et al.*[65] and more recently discussed by Lemaitre and Caroli[64], each local slip induces a stress fluctuation whose amplitude is proportional to d , which can be seen accordingly as an effective mechanical temperature. Following this interpretation, the higher d , the higher the mechanical noise and the lower the external stress needed to destabilize a shear zone. A clear limit of this interpretation is the high degree of spatial correlation of the elastic response to a local slip. Without pursuing further this interpretation, let us simply note that the systematic decrease of the plateau stress with the slip increment d observed in Fig. 3 follows qualitatively this picture.

In Fig. 4a we show hardening curves obtained for a system of size $L = 256$ with values of the slip increment parameter ranging from $d = 0.01$ to $d = 1$. We then test in Fig. 4b a simple rescaling using the reduced variables $\langle \Sigma \rangle / \Sigma_Y$ and $\langle \varepsilon_p \rangle / \varepsilon_{0.5}$ where Σ_Y is the plateau stress value and $\varepsilon_{0.5}$ is the plastic strain obtained at $\Sigma = 0.5\Sigma_Y$. While not perfect the superimposition obtained with this procedure is reasonable and appears to gain in quality for small values of d . In Fig. 4c we show the scaling behavior of the plateau stress σ_Y and the typical plastic strain $\varepsilon_{0.5}$. The latter shows a sublinear dependence to d , $\varepsilon_{0.5} \propto d^{0.85}$ while the former approaches unity, the upper limit of the threshold distribution with a close to square root dependence $1 - \Sigma_Y \propto d^{0.48}$.

A naive view of this behavior (leading to a square root scaling for both quantities) consists of noting that small values of d allows for a more precise exploration of the valleys of the disordered landscape. Multiple slips at the location are thus necessary before plastic activity jumps to another site. Since any time, a slip occurs, the internal stress is incremented by an elastic response of order d , the typical deformation can be seen as a first return of a biased random walk of slope d .

The initial curvature of the stress/strain response is characteristic of a transient hardening behavior, also called micro-plasticity *i.e.* the progressive increase of the yield stress upon deformation. Such a phenomenon, traditionally attributed to dislocation entanglement or pinning by impurities in metal plasticity was first believed to be absent in amorphous plasticity[11]. Yet, the phenomenon of progressive densification of silicate glasses upon high pressure cycling can be interpreted as density hardening effect[74]. Moreover a clear effect of strain hardening upon shear cycling

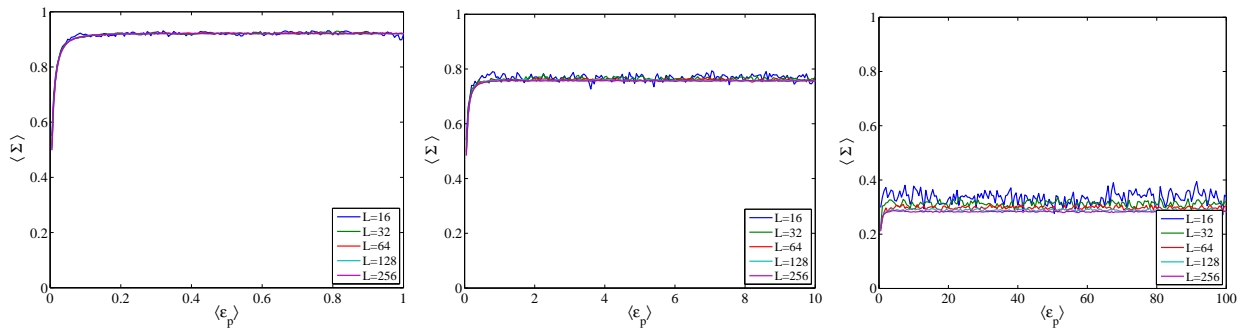


FIG. 3: Hardening curves: Averaged stress $\langle \Sigma \rangle$ vs. plastic strain ε obtained for three values of the d parameter. ($d = 0.01$ left, $d = 0.1$ center and $d = 1$ right). The curvature signs a clear hardening effect, *i.e.* the elastic limit (yield stress) increases with plastic strain. After the hardening stage, the stress saturates at a plateau value, the macroscopic yield stress Σ_Y .

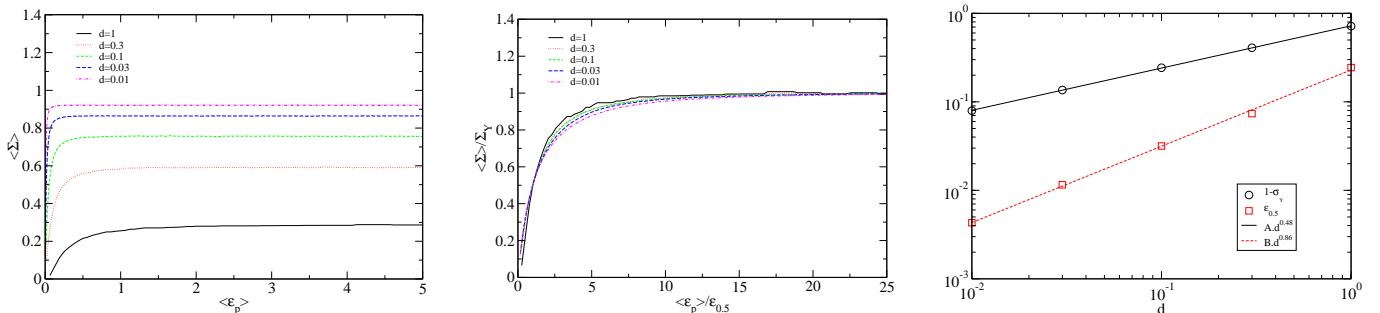


FIG. 4: Left: Averaged stress $\langle \Sigma \rangle$ vs. plastic strain ε obtained for a system of size $L = 256$ with values of the slip increment parameter ranging from $d = 0.01$ to $d = 1$. Center: same data after rescaling by the plateau stress value Σ_Y and the plastic strain $\varepsilon_{0.5}$ obtained at $\langle \Sigma \rangle = 0.5 \Sigma_Y$. Right: Evolution of the plateau stress Σ_Y and the typical plastic strain $\varepsilon_{0.5}$ with the slip increment d .

has been reported recently[75]. Within the present model, it is possible to give a simple statistical interpretation of strain hardening phenomenon in absence of dislocations. As early discussed in Ref. [57] the increase of the yield stress can be related to the progressive exhaustion of the weakest spots of the materials.

This phenomenon is clearly visible in Fig. 5 where we represented the evolution under shear of the distribution of local thresholds $P(\sigma_\gamma)$ and of the distribution of residual elastic stress $P(\sigma_{el})$. While originally uniform in the interval $[0, 1]$, the distribution of plastic thresholds is progressively shifted toward high values by exhaustion of the weakest sites before reaching a limit steady state distribution. In the transient regime, a self-organized-critical-like dynamics seems at work: weak sites are replaced by normal ones, thus inducing a systematic bias to the distribution. While less remarkable a similar trend may be extracted from the evolution of the stress distribution. A clear asymmetry is visible: large positive stress values which favor local reorganization are less frequent than their negative counterparts.

IV. A NON-PERSISTENT LOCALIZING BEHAVIOR

By the very definition of the model, the mean plastic strain increases in proportion to the number of events, or “time”. As the mean plastic strain increases, the macroscopic stress reaches a plateau in the steady state, $\langle d\sigma \rangle / d\varepsilon = 0$. Using classical results from continuum mechanics, for homogeneous media, the system is at the limit between a hardening behavior $d\sigma / d\varepsilon > 0$, expected to give rise to a homogeneous plastic strain, and a softening regime $d\sigma / d\varepsilon < 0$ where strain should localize. A simple way to illustrate this property, is to note that a uniform (but of arbitrary magnitude) slip along a line oriented at $\pm\pi/4$ with respect to the principal axes, will not induce any stress in the medium. Introducing $\mathbf{n}_1 = 1/\sqrt{2}(1, 1)$ and $\mathbf{n}_2 = 1/\sqrt{2}(1, -1)$, and arbitrary scalar functions f and g ,

$$\varepsilon_p(\mathbf{x}) = f(\mathbf{x} \cdot \mathbf{n}_1) + g(\mathbf{x} \cdot \mathbf{n}_2) \quad (8)$$

is a field which does not involve any elastic stress within the medium. In our model, the residual elastic stress is the only way to endow the system with memory, and hence, no limiting (nor amplifying) mechanism will act against (with) such degrees of freedom.

A. Fluctuations of plastic strain

The presence of disorder gives rise to stress fluctuations around the average, which may affect this simple picture, and hence it is of interest to characterize the inhomogeneity of the plastic strain field. A first simple estimator is the standard deviation of the entire plastic strain field,

$$\delta\varepsilon_p = [\langle\varepsilon_p^2\rangle - \langle\varepsilon_p\rangle^2]^{1/2} \quad (9)$$

which is to be characterized as a function of the mean plastic strain $\langle\varepsilon_p\rangle$. Indeed, on the one hand, for a plastic strain field which does not display any long range correlation, $\delta\varepsilon_p$, should saturate to a constant, independent of $\langle\varepsilon_p\rangle$ and L . If, on the other hand, the plastic strain is localized on a simple slip system (a straight line spanning the entire system), then along this localization band, namely for L sites, the plastic strain amounts to $\varepsilon_1 = L\langle\varepsilon_p\rangle$, whereas it is null over the rest of the system. In this case, the standard deviation amounts to $\delta\varepsilon_p \propto L^{1/2}\langle\varepsilon_p\rangle$. Therefore the scaling of $\delta\varepsilon_p$ with L and $\langle\varepsilon_p\rangle$ is informative on the more or less uniform distribution of plastic strain.

The evolution of the variance of the plastic strain as a function of the mean strain is shown in Fig. 6a in a log-log plot for systems of size $L = 128$ and various values of the slip increment parameter ranging from $d = 0.01$ to $d = 1$. A reasonable collapse onto a master curve can be obtained when using the reduced plastic strain $\varepsilon_p/d^{1/2}$. As discussed above the quality of the rescaling procedure increases when the value of d decreases.

A transient power-law like regime can be identified. An indicative straight line of slope 0.7 is shown in the transient regime. Then the strain fluctuation seem to slowly transit toward a diffusive like regime. Again an indicative straight line of slope 0.5 is shown in this regime.

Coming back to the above discussion we thus obtain a power law evolution of the standard deviation of strain $\delta\varepsilon_p \propto \langle\varepsilon_p\rangle^\alpha$ with an exponent $\alpha \approx 0.7$ in the transient regime and $\alpha \approx 0.5$ in a second diffusive-like regime. These results are thus intermediate between a homogeneous deformation regime and a full localization behavior. In Fig. 6b we represent the evolution of the elastic stress variance. The contrast with plastic strain fluctuation is striking since we observe here a clear saturation after the transient regime. This means that plastic strain is dominated by stress free soft modes $\pm 45^\circ$. These results help us to give a first picture of the behavior of the system. After spatial correlations have been established in a transient localized regime (high value of the exponent α), the system transits toward a diffusive regime where plastic deformation can be seen as a random succession of shear bands in the directions at $\pm 45^\circ$.

B. Plastic stress and strain field maps

Beyond this macroscopic behavior, a closer look at the local scale gives evidence for the development of strong spatial correlations. Fig. 7 presents a series of maps of plastic activity at different levels of mean plastic strain. Every map corresponds to the plastic strain accumulated during a finite strain window $\Delta\varepsilon_p = 0.01$. While the plastic

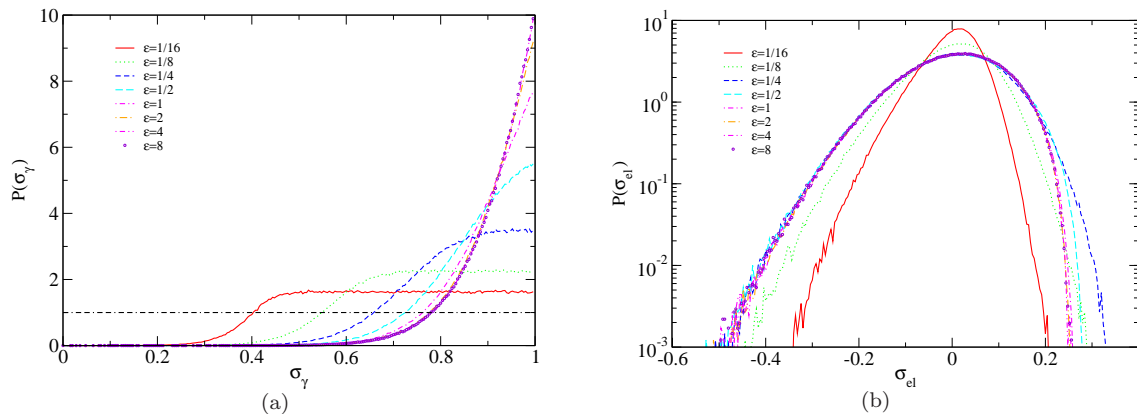


FIG. 5: Evolution of (a) the distribution of microscopic plastic thresholds and (b) the distribution of internal stress under plastic strain. Data are obtained with a system of size $L = 64$ with a slip increment parameter $d = 0.1$, averaged over 250 realizations. Due to the exhaustion of weak sites, the distribution of thresholds progressively shifts toward high values and converges toward a limit distribution of typical width d . The internal stress distribution (here represented in semi-log coordinates) converges toward a Gaussian-like distribution with however a notable asymmetry: a fatter tail for the negative stress.

activity is initially homogeneously distributed in space, the progressive development of correlations along the \mathbf{n}_1 and \mathbf{n}_2 directions. Simultaneously, it appears that larger and larger regions remain still, i.e. without any plastic flow. As earlier noted, plastic strain appears as streaks aligned with either \mathbf{n}_1 or \mathbf{n}_2 . Let us note that these patterns observed at the largest scale generate little stresses as they can grossly be described by the modes described in Eq. 8.

Note that this localization appears not to be persistent. While the incremental plastic strain displays similar patterns at different times, shear bands are not superimposed, but they rather move through the system with statistically similar features past the initial transient at different deformation levels; they seem to diffuse in the system. The two left panels of Fig. 8 where we represented the plastic activity at $\varepsilon = 0.95$ and $\varepsilon = 1.0$ give an illustration of this competition between localization and diffusion. In the second map, we recover hints of the first one but most of the plastic activity has moved elsewhere. The last panel of Fig. 8 proposes a striking comparison with recent numerical results by Maloney and Robbins[33, 39]. These authors study the behavior of a two-dimensional Lennard-Jones glass under uni-axial compression, and periodic boundary condition for the stress and strain field, a situation which is quite comparable to our own boundary conditions. They show the vorticity of the displacement field, in order to highlight the zones of concentrated plastic strain. With this representation, a slip line along the \mathbf{n}_1 (resp. \mathbf{n}_2) direction appears as a line of concentrated negative (resp. positive) vorticity, whereas the local density of plastic strain does not distinguish between both directions.

The concentration of strain over lines in the direction of maximum shear is reminiscent also of the (left) SEM image shown in Fig. 1 (Note that the right image corresponds to an anti-plane situation such as the one addressed in Baret et al[57]). The specimen shown in this figure however has a very large size (2 mm diameter), and slip amplitudes on major slip planes are in the micrometer range. This involves other phenomena (heat dissipation, and softening) which are not taken into account here. Nevertheless, the initiation of multiple localization (rather than a uniform strain field) may be argued to be of a similar origin as the large scale localization of the present model.

The growth of the correlation length takes place in the initial transient up to the stage where it reaches the system size, and steady state is established. Up to now, we essentially focused on this initial stage. However, since we observed the formation of large scale structures, it is of interest to characterize the signature of the largest structures in the steady state. In the following sections space correlations in the stress and plastic strain fields are discussed.

In contrast to the plastic strain which can grow without limit, stress is here bounded. Figure 9(left) shows a typical stress map obtained in the steady state for a system of size $L = 128$ and $d = 0.01$. No specific feature can be perceived on such maps. However, because of the preferential orientation of plastic events at $\pm\pi/4$, it is to be expected that the stress field display a similar anisotropic signature. The power spectrum of the stress field shown on Figure 9(right) indeed reveal that the power spectra along such preferential directions are considerably depressed as compared to other directions.

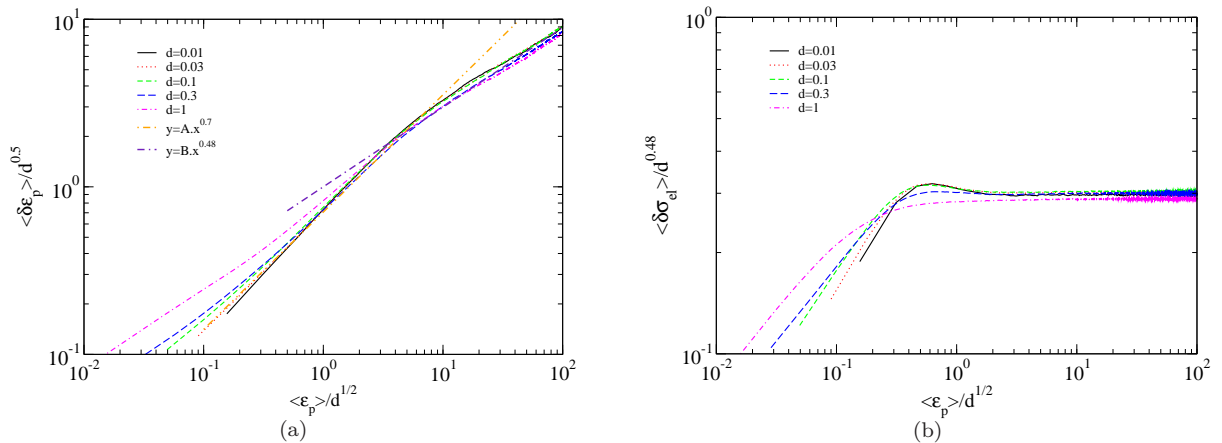


FIG. 6: (a) Log-log plot of the evolution of the rescaled standard deviation of plastic strain $\delta\varepsilon_p/d^{0.5}$ with rescaled plastic strain $\langle\varepsilon_p\rangle/d^{0.5}$ ($L = 128$, $d = 0.01, 0.03, 0.1, 0.3, 1$). A dotted line of slope 0.7 is shown as a reference in the transient regime, and a dot-dashed line of slope unity is shown in the “stationary” regime. (b) Evolution of the rescaled residual stress standard deviation $\delta\sigma_{el}/d^{0.48}$ in the same coordinates. In contrast with strain, a real saturation regime can be identified.

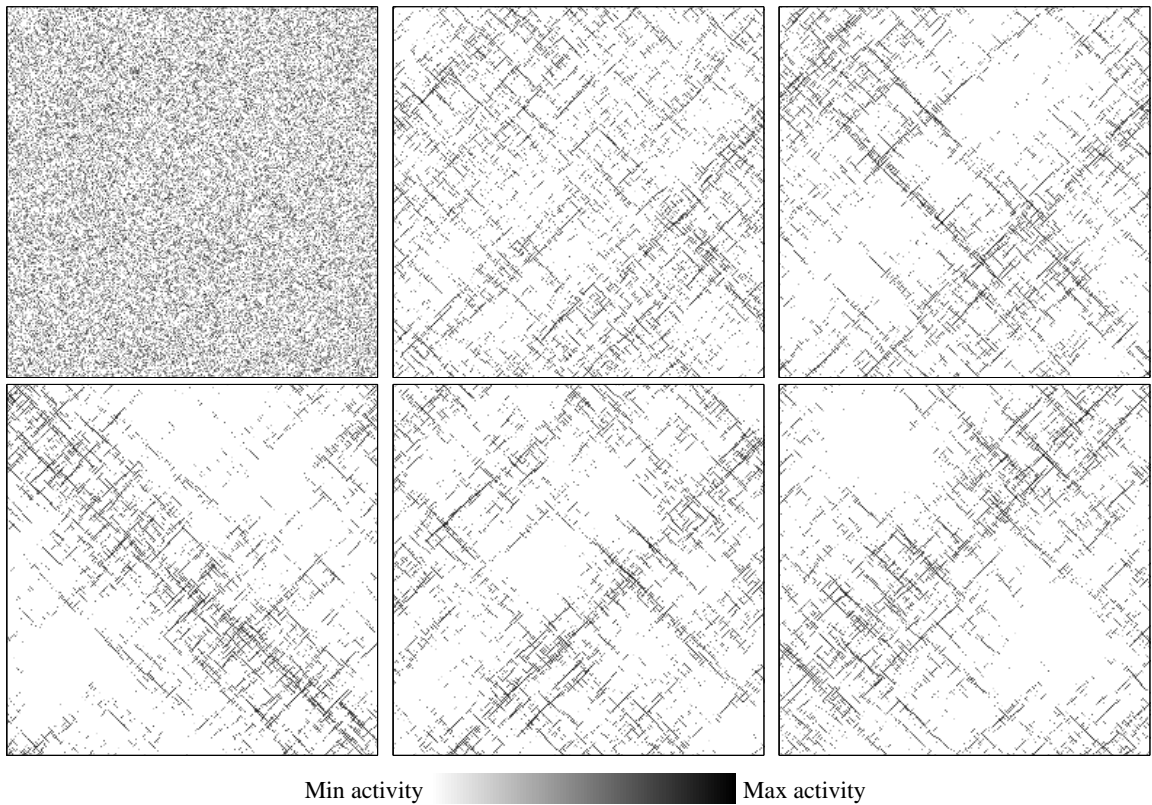


FIG. 7: Maps of cumulated plastic activity during “time” windows corresponding to increasing levels of deformation: $\varepsilon = 0.01, 0.10, 0.20, 0.30, 0.50, 1.00$. The system size is $L = 256$. While random at the beginning, the plastic activity progressively localizes along \mathbf{n}_1 and \mathbf{n}_2 directions.

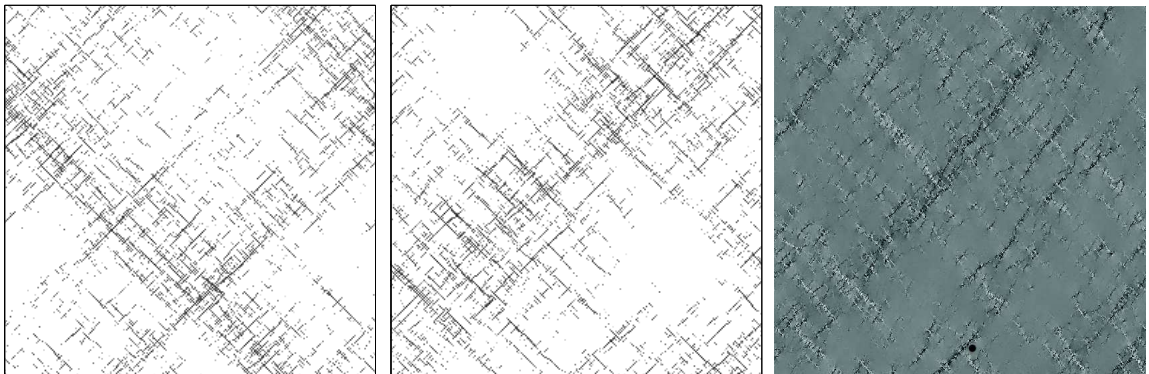


FIG. 8: Left: Map of cumulated plastic activity during a “time” window corresponding to a duration $\Delta\varepsilon = 0.01$ taken at $\varepsilon = 0.95$ with $L = 256$, $d = 0.01$. A clear localization of the plastic deformation is observed. Center: same as Left but taken “later” at $\varepsilon = 1.0$. Again plasticity localizes along elongated structures at $\pm 45^\circ$ but the patterns are markedly different: localization is not persistent. Right: for comparison, reproduction of a strikingly similar map of plastic activity (vorticity of the displacement field) recently obtained by Maloney and Robbins[39]) on a 2D Lennard-Jones glass under compression.

V. ANISOTROPIC STRAIN CORRELATIONS

We now give a quantitative analysis of the anisotropic plastic strain correlations. A first method consists in considering the spatial distribution of successive plastic events $P(\Delta\mathbf{x})$. A map of this distribution is presented in Fig. 10(a) for the upper right quadrant. Without surprise, we obtain a panache that obeys the quadrupolar symmetry of the elastic kernel: a plastic event is far more probable in a direction at $\pm\pi/4$ degree than along the principal axis. The width of this panache can be quantified. Fig. 10(b) shows the standard deviation $sd_{\Delta y}$ of the distance Δy for a

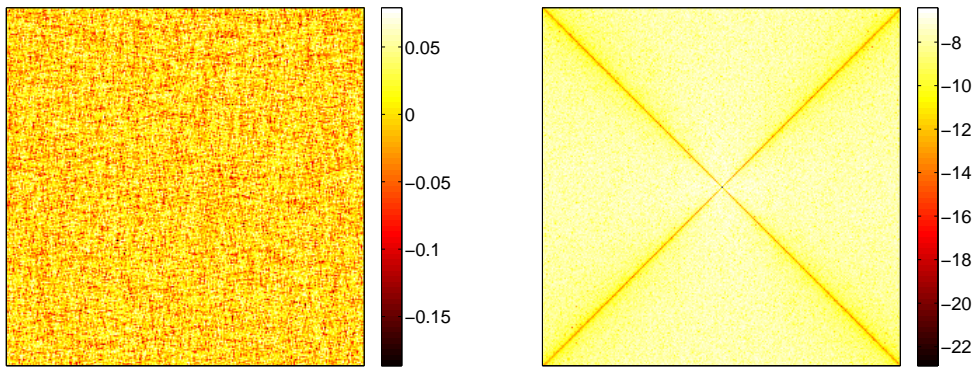


FIG. 9: (left) Stress map in the steady state, $L = 256$, $d = 0.01$. (right) Power spectrum (logarithmic color scale) of the stress map.

d	0.01	0.1	1
α_0	0.33	0.32	0.27
$\alpha_{\pi/4}$	1.67	1.75	1.71

TABLE I: Scaling exponents of anisotropic strain power spectrum for different values of the strain increment $d = 0.01, 0.1, 1$

given value of the distance Δx between two successive plastic events. We obtain a nice scaling relation $sd_{\Delta y} \propto \Delta x^\zeta$ where $\zeta \approx 0.65$. Note that a similar value was obtained in the anti-plane shear case discussed in Ref. [57]. Such a value corresponds also to the roughness exponent of minimal path in a random potential [76] which can easily be proven to be relevant for anti-plane plasticity with quenched random yield stress. The fact that the value of this exponent is less than unity indicates an important property of the plastic strain patterns: the aspect ratio decreases as $\Delta x^{\zeta-1}$ so that asymptotically, shear is concentrated on straight bands of vanishing relative width.

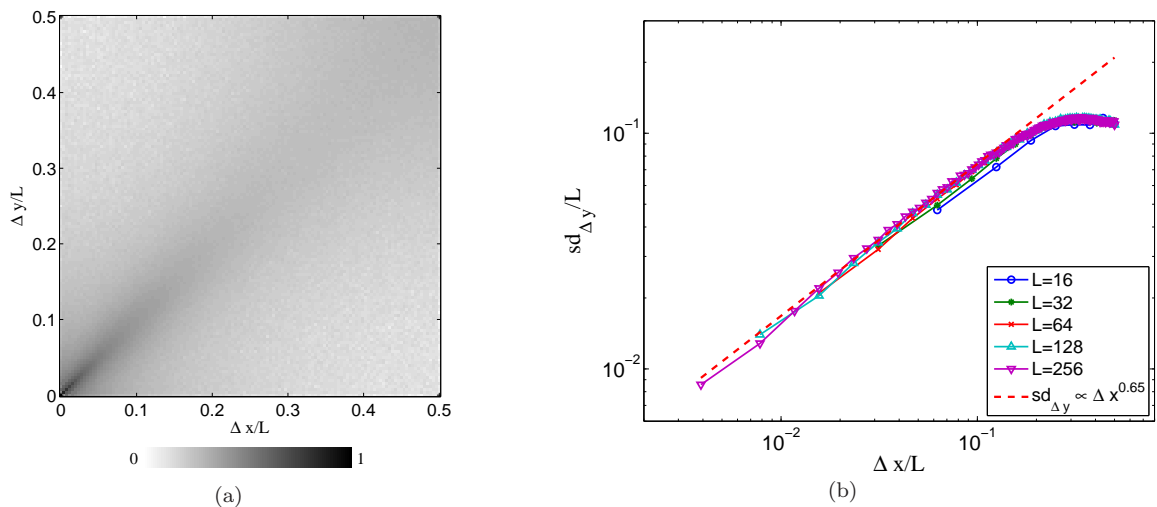


FIG. 10: (a) Map of $P(\Delta x, \Delta y)$, the probability that two successive plastic events are separated by distances Δx and Δy along x - and y -axis for a system of size $L = 256$. Preferential angles at $\pm\pi/4$ are clearly visible. (b) Standard deviation $sd_{\Delta y}$ of the separation of two consecutive plastic events along the y -axis for a given value of the separation distance Δx . A power law behavior $sd_{\Delta y} \propto \Delta x^\zeta$ is obtained with $\zeta \approx 0.65$. The fact that $\zeta < 1$ shows that the relative width of those shear bands tends to 0 for large system sizes.

In order to characterize the correlations of the plastic strain field, the most natural analysis is to compute the power spectrum of the plastic strain field. In Fig. 11(left), an ensemble average of 2D power spectra of the strain field is shown. This map, here encoded in logarithmic scale, exhibits a marked fourfold symmetry, with obvious preferential directions along \mathbf{n}_1 and \mathbf{n}_2 . To be more quantitative, we now consider the scaling of power spectra cuts along the preferred directions and along the principal axes, as shown in Fig. 11(right). As summarized in Table I for power

spectra obtained with different values of the strain increment d , both of these spectra can be characterized by a power-law behavior with exponents $\alpha_{\pi/4} \approx 1.7$, $\alpha_0 \approx 0.3$ where the indices denote the orientation of the wave vector with respect to the x -axis. Such behaviors can equivalently be characterized as self-affine, with respective roughness exponents $\zeta_{\pi/4} \approx 0.35$ and $\zeta_0 \approx -0.35$. It is however to be emphasized that the most important feature of power spectra along directions $\theta \neq \pm\pi/4$, is that their magnitude is orders of magnitude lower than for $\theta \pm \pi/4$.

In the case of anti-plane shear, a previous study [57] also revealed an anisotropic plastic strain field in the steady state. In that case, the power spectra of ε_p showed a different scaling with the wave-number parallel or perpendicular to the orientation of the shear band.

In their recent study of a Lennard-Jones glass under compression [33, 39], Maloney and Robbins discussed the anisotropic scaling of plastic strain. As shown in Fig. 8, when representing the vorticity of the displacement field, they obtained maps of plastic activity strikingly similar to ours. Looking at the correlation of the vorticity they obtained a power spectrum with a four-fold symmetry:

$$S(q, \theta) \propto a(\theta)q^{-\alpha(\theta)}, \quad \alpha(\theta) = 0.68 - 0.5 \cos(4\theta) \quad (10)$$

and thus in particular $\alpha_{\pi/4} = 1.18$ and $\alpha_0 = 0.18$, to compare to the above reported values. In the latter expression, $a(\theta)$ is unspecified.

Considering the power spectra of the cumulated plastic strain, we expect to observe a directly comparable quantity. Indeed, we do observe a direction dependent scaling exponent. In Fig. 11 we reported the scaling behavior obtained along cuts in different directions while the angular dependence of $S(q, \theta)$ is shown in Fig. 12. Again most of the plastic activity appears to be concentrated along the directions at $\pm\pi/4$. Except in the close vicinity of that preferred direction, the value of the scaling exponent remains close to α_0 , and only shows a slow increase when the direction of the cut approaches the diagonal.

Representing part of the same results as a function of the polar angle, we observe that an equation comparable to the previous, gives a good account of our data

$$S(q, \theta) = A (q/q_0)^{-\alpha(\theta)}, \quad \alpha(\theta) = \alpha_{\pi/4} - (\alpha_{\pi/4} - \alpha_0) |\cos(2\theta)|^{0.4} \quad (11)$$

where we considered the case $d = 0.01$. The angular dependency of the power spectrum is written in a slightly different manner, but both share the same fourfold symmetry. At a fixed wavevector modulus, Eq. 11 proposes an amplitude of $Aq_0^\alpha(\theta)$ whereas Maloney and Robbins propose $A(\theta)$. However the difference is marginal, as the lower exponents correspond to much smaller amplitudes.

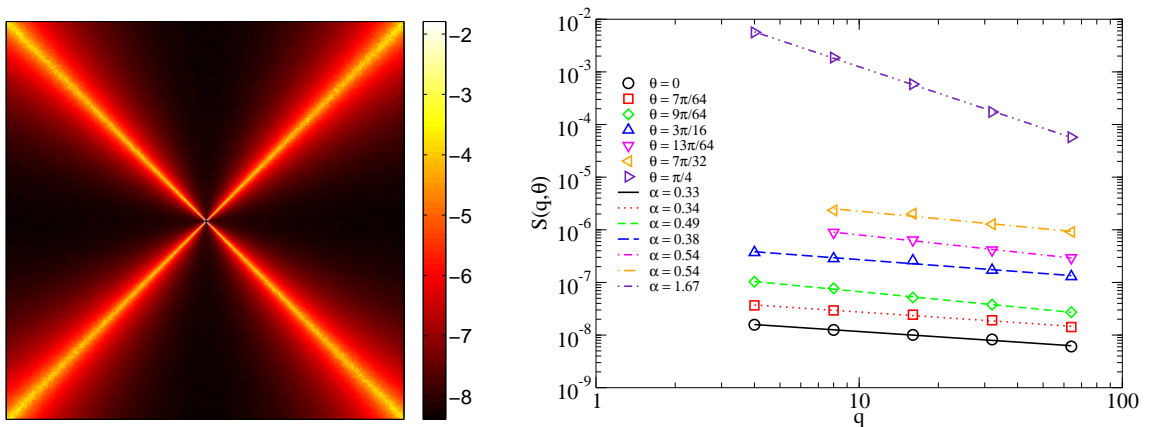


FIG. 11: (a) Power spectrum of the plastic strain using a decimal log scale. A clear quadrupolar symmetry is obtained. (b) Cuts along the axis at $\theta = 0$ and $\theta = \pi/4$. Different power law behaviors $S(q) \propto q^{-\alpha}$ are obtained between the extreme cases $\alpha_0 \approx 0.33$ and $\alpha_{\pi/4} \approx 1.67$. $L = 256$ and $d = 0.01$.

VI. INFLUENCE OF INITIAL STATE

While the richness of the physics of depinning models mainly relies on the competition between elasticity and disorder, we see here that the anisotropic character and the abundance of soft modes in the elastic interaction

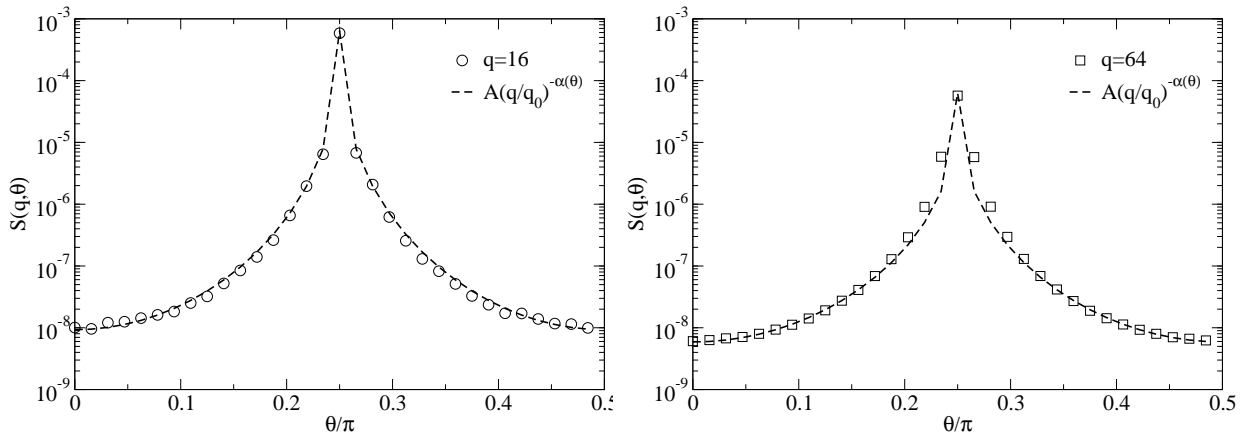


FIG. 12: Angular dependence of the power spectrum obtained for two values of the wavenumber: $q = 16$ (Left) and $q = 64$ (Right) with the parameters $L = 256$, $d = 0.01$. The symbols represent the numerical data; The dashed lines corresponds to the best fit obtained with a scaling form $s(q, \theta) \propto A(q/q_0)^{-\alpha(\theta)}$ with an exponent $\alpha(\theta) = 1.67 - 1.34|\cos(2\theta)|^{0.4}$ exhibiting a quadrupolar symmetry.

which characterize the present model of amorphous plasticity, naturally induce an additional competition between localization and disorder.

An implicit hypothesis performed in our model is that the statistical distribution used to renew the local plastic threshold under shear (*i.e.* after local slip) is the very same as the distribution of plastic thresholds in the initial configuration. The evidence of this hypothesis may be questioned. Indeed, various experimental and numerical results obtained in friction or in shearing granular material or complex fluids [32, 77, 78] seem to show an effect of the preparation of the material upon its behavior under shear. One may think for instance at the effect of density of granular material: a loose (dense) packing tends to exhibit hardening (softening) while under shear their density progressively evolves toward a “critical” value. In order to test the effect of our hypothesis we give in the following a bias to the initial thresholds distribution and try to test its consequences. Practically speaking the initial thresholds are drawn from a uniform distribution in the range $[\zeta_0, 1 + \zeta_0]$ while the (uniform) distribution of renewed threshold remains unchanged in the range $[0, 1]$. A positive (negative) value of ζ_0 is expected to induce some softening (hardening) behavior since all threshold values above unity (below zero) should eventually be replaced by thresholds within the interval $[0, 1]$. We show below results obtained with a system of size $N = 128$, a maximum slip increment $d = 1$ and a bias $\zeta_0 = 0.5$. The effect appears to be rather spectacular since as shown in Fig. 13 a clear persistent localization is now obtained.

Let us only note here that the way the plastic activity gets localized along a band is somewhat reminiscent of the behavior of an earlier model proposed by Torok and Roux [79]. In this study, the authors made evidence for a weak breaking of ergodicity which they relate to the progressive building in the thresholds landscape of a valley (along the shear band) surrounded by ridges elevating significantly above the base level. Plastic activity thus tends to be confined in the valley and can no longer fully explore the disordered landscape.

VII. CONCLUSIONS

The plasticity of amorphous media was addressed through a meso-scale modeling in order to highlight the large scale mechanical behavior. This modeling was constructed in order to retain the most important features of a macroscopic description and compared favorably with much richer descriptions. The macroscopic behavior tends to approach an elastic/perfectly plastic law. The progressive approach to a constant yield stress is interpreted as a statistical selection of high threshold local configuration. In the perfect plasticity regime, strain tends to localize along the direction of maximum shear as could have been anticipated. However, the fact that elementary plastic events are localized in space give rise to specific features in the spatial correlation of plastic strains (with self-similar power spectra), and fluctuations of macroscopic yield stress occurring at large scales. Finally, the influence of the initial state of the medium has been shown to favor an early localization of the strain onto a unique and persistent shear band.

The present model can also be regarded as a depinning model, (comparable to the ones introduced for elastic lines or membranes[61]). The associated critical aspects of the model, in particular its (non mean-field)avalanche behavior will be discussed elsewhere[80].

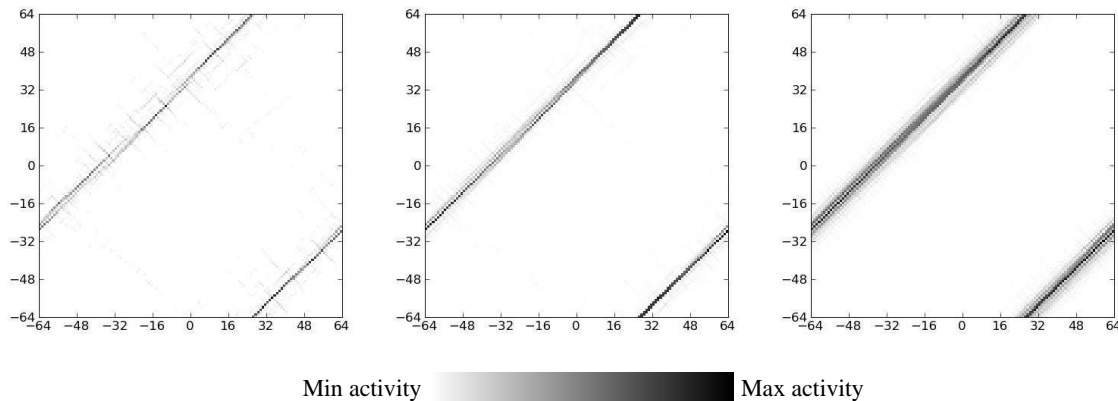


FIG. 13: Maps of total cumulated plastic activity corresponding to increasing levels of deformation: $\varepsilon = 0.25, 1.0, 4.0$. The initial threshold distribution is here shifted by $\zeta_0 = 0.5$. The system size is $L = 128$. A clear persistent shear band can be observed.

An extension accounting for the coupling between deviatoric and volumetric strain remains to be investigated. It would also allow to study the hardening behavior while paying attention to the potential apparition of an anisotropic texture as recently discussed in [37].

While it is the most classical macroscopic observable the hardening curve only gives us the evolution of mean quantities. Until recently, only such integrated quantities were experimentally accessible through the use of strain gauges and force sensors. The recent development of “digital image correlation” has allowed one the direct access to two-dimensional and even three-dimensional displacement fields. In the particular field of mechanics of disordered materials, these promising techniques thus give the possibility to follow the fluctuations of the strain field and more generally the development of its spatio-temporal correlations and to compare them with model predictions.

Acknowledgments

We are thankful to Jing Zhang and Patrick Amedieu for the SEM images shown in Fig. 1. C.E. Maloney and M.O. Robbins for the authorization of replicating their figure in Fig. 8 from Ref. [39].

-
- [1] E. W. Taylor, *Nature* **163**, 323 (1949).
 - [2] D. M. Marsh, *Proc. Roy. Soc. A* **279**, 420 (1964).
 - [3] P. W. Bridgman and I. Simon, *J. Appl. Phys* **24**, 405 (1953).
 - [4] H. M. Cohen and R. Roy, *J. Am. Ceram. Soc.* **44**, 523 (1961).
 - [5] J. D. Mackenzie, *J. Am. Ceram. Soc.* **46**, 461 (1963).
 - [6] F. M. Ernsberger, *J. Am. Ceram. Soc.* **51**, 545 (1968).
 - [7] K. W. Peter, *J. Non-Cryst. Sol.* **5**, 103 (1970).
 - [8] S. Yoshida, T. Rouxel, and J.-C. Sangleboeuf, *J. Mater. Res.* **55**, 1159 (2006).
 - [9] A. Perriot, V. Martinez, C. Martinet, B. Champagnon, D. Vandembroucq, and E. Barthel, *J. Am. Ceram. Soc.* **89**, 596 (2006).
 - [10] G. Kermouche, E. Barthel, D. Vandembroucq, and P. Dubujet, *Acta Mat.* **56**, 3222 (2008).
 - [11] C. A. Schuh, T. C. Hufnagel, and U. Ramamurty, *Acta. Mat.* **55**, 4067 (2007).
 - [12] J. Zhang, P. Amedieu, F. Hild, S. Roux, and T. Zhang, *Scripta Mat.* **61**, 1145 (2009).
 - [13] M. L. Falk and J. S. Langer, *Phys. Rev. E* **57**, 7192 (1998).
 - [14] J. Rottler and M. O. Robbins, *Phys. Rev. E* **64**, 051801 (2001).
 - [15] A. Tanguy, J. P. Wittmer, F. Leonforte, and J.-L. Barrat, *Phys. Rev. B* **66**, 174205 (2002).
 - [16] J. Rottler and M. O. Robbins, *Phys. Rev. E* **68**, 011507 (2003).
 - [17] A. C. Lund and C. A. Schuh, *Acta. Mat.* **51**, 5399 (2003).
 - [18] F. Varnik, L. Bocquet, J.-L. Barrat, and L. Berthier, *Phys. Rev. Lett.* **90**, 095702 (2003).
 - [19] M. J. Demkowicz and A. S. Argon, *Phys. Rev. Lett.* **93**, 025505 (2004).
 - [20] C. E. Maloney and A. Lemaître, *Phys. Rev. Lett.* **93**, 016001 (2004).
 - [21] C. E. Maloney and A. Lemaître, *Phys. Rev. Lett.* **93**, 195501 (2004).

- [22] F. Leonforte, A. Tanguy, J. P. Wittmer, and J.-L. Barrat, *Phys. Rev. B* **70**, 014203 (2004).
- [23] F. Varnik, L. Bocquet, and J.-L. Barrat, *J. Chem. Phys.* **120**, 2788 (2004).
- [24] M. J. Demkowicz and A. S. Argon, *Phys. Rev. B* **72**, 245205 (2005).
- [25] M. J. Demkowicz and A. S. Argon, *Phys. Rev. B* **72**, 245206 (2005).
- [26] Y. F. Shi and M. L. Falk, *Phys. Rev. Lett.* **95**, 095502 (2005).
- [27] F. Leonforte, R. Boissiere, A. Tanguy, J. P. Wittmer, and J.-L. Barrat, *Phys. Rev. B* **72**, 224206 (2005).
- [28] Y. F. Shi and M. L. Falk, *Phys. Rev. B* **73**, 214201 (2006).
- [29] C. E. Maloney and A. Lemaître, *Phys. Rev. E* **74**, 016118 (2006).
- [30] A. Tanguy, F. Leonforte, and J.-L. Barrat, *Eur. Phys. J. E* **20**, 355 (2006).
- [31] F. Leonforte, A. Tanguy, J. P. Wittmer, and J.-L. Barrat, *Phys. Rev. Lett.* **97**, 055501 (2006).
- [32] Y. F. Shi, M. B. Katz, H. Li, and M. L. Falk, *Phys. Rev. Lett.* **98**, 185505 (2007).
- [33] C. E. Maloney and M. O. Robbins, *J. Phys. Cond. Matt.* **20**, 244128 (2008).
- [34] M. Tsamados, A. Tanguy, F. Leonforte, and J.-L. Barrat, *Eur. Phys. J. E* **26**, 283 (2008).
- [35] M. Tsamados, A. Tanguy, C. Goldenberg, and J.-L. Barrat, *Phys. Rev. E* **80**, 026112 (2009).
- [36] M. Talati, T. Albaret, and A. Tanguy, *Europhys. Lett.* **86**, 66005 (2009).
- [37] C. L. Rountree, D. Vandembroucq, M. Talamali, E. Bouchaud, and S. Roux, *Phys. Rev. Lett.* **102**, 195501 (2009).
- [38] A. S. Argon, *Acta Metall.* **27**, 47 (1979).
- [39] C. E. Maloney and M. O. Robbins, *Phys. Rev. Lett.* **102**, 225502 (2009).
- [40] A. Lemaître and C. Caroli, *Phys. Rev. Lett.* **103**, 065501 (2009).
- [41] E. Lerner and I. Procaccia, *Phys. Rev. E* **80**, 026128 (2009).
- [42] D. J. Lacks, *Phys. Rev. Lett.* **80**, 5385 (1998).
- [43] W. Jin, R. K. Kalia, P. Vashishta, and J. P. Rino, *Phys. Rev. Lett.* **71**, 3146 (1993).
- [44] W. Jin, R. K. Kalia, P. Vashishta, and J. P. Rino, *Phys. Rev. B* **50**, 118 (1994).
- [45] D. J. Lacks, *Phys. Rev. Lett.* **84**, 4629 (2000).
- [46] L. P. Dávila, M. J. Caturla, A. Kubota, B. Sadigh, T. D. de la Rubia, J. F. Shackelford, S. H. Risbud, and S. H. Garofalini, *Phys. Rev. Lett.* **91**, 205501 (2003).
- [47] A. Rahmani, M. Benoit, and C. Benoit, *Phys. Rev. B* **68**, 184202 (2003).
- [48] L. Huang and J. Kieffer, *Phys. Rev. B* **69**, 224203 (2004).
- [49] L. Huang and J. Kieffer, *Phys. Rev. B* **69**, 224204 (2004).
- [50] Y. Liang, C. R. Miranda, and S. Scandolo, *Phys. Rev. B* **75**, 024205 (2007).
- [51] C. Goldenberg, A. Tanguy, and J.-L. Barrat, *Europhys. Lett.* **80**, 16003 (2007).
- [52] E. Lerner and I. Procaccia, *Phys. Rev. E* **79**, 066109 (2009).
- [53] V. V. Bulatov and A. S. Argon, *Modell. Simul. Mater. Sci. Eng.* **2**, 167 (1994).
- [54] V. V. Bulatov and A. S. Argon, *Modell. Simul. Mater. Sci. Eng.* **2**, 185 (1994).
- [55] V. V. Bulatov and A. S. Argon, *Modell. Simul. Mater. Sci. Eng.* **2**, 203 (1994).
- [56] E. R. Homer and C. A. Schuh, *Acta Mat.* **57**, 2823 (2009).
- [57] J.-C. Baret, D. Vandembroucq, and S. Roux, *Phys. Rev. Lett.* **89**, 195506 (2002).
- [58] K. Chen, P. Bak, and S. P. Obukhov, *Phys. Rev. A* **43**, 625 (1991).
- [59] Y. Ben-Zion and J. R. Rice, *J. Geophys. Res.* **98**, 14109 (1993).
- [60] O. Narayan and D. S. Fisher, *Phys. Rev. B* **48**, 7030 (1993).
- [61] M. Kardar, *Phys. Rep.* **301**, 85 (1998).
- [62] G. Picard, A. Ajdari, F. Lequeux, and L. Bocquet, *Phys. Rev. E* **71**, 010501(R) (2005).
- [63] L. Bocquet, A. Colin, and A. Ajdari, *Phys. Rev. Lett.* **103**, 036001 (2009).
- [64] A. Lemaître and C. Caroli, *arxiv:cond-mat/0609689v1* (2006).
- [65] P. Sollich, F. Lequeux, P. Hébraud, and M. E. Cates, *Phys. Rev. Lett.* **78**, 2020 (1998).
- [66] E. A. Jagla, *Phys. Rev. E* **76**, 046119 (2007).
- [67] T. Ooshida and K. Sekimoto, *Phys. Rev. Lett.* **95**, 108301 (2005).
- [68] M. Zaiser and P. Moretti, *J. Stat. Mech.* **P08004**, 79 (2005).
- [69] K. A. Dahmen, Y. Ben-Zion, and J. T. Uhl, *Phys. Rev. Lett.* **102**, 175501 (2009).
- [70] F. Delogu, *Phys. Rev. Lett.* **100**, 255901 (2008).
- [71] D. Rodney and C. A. Schuh, *Phys. Rev. Lett.* **102**, 235503 (2009).
- [72] D. MacNeill and J. Rottler, *Phys. Rev. E* **81**, 011804 (2010).
- [73] M. Talamali, V. Petäjä, D. Vandembroucq, and S. Roux, *Phys. Rev. E* **78**, 016109 (2008).
- [74] D. Vandembroucq, T. Deschamps, C. Coussa, A. Perriot, E. Barthel, B. Champagnon, and C. Martinet, *J. Phys. Cond. Mat.* **20**, 485221 (2008).
- [75] C. E. Packard, L. M. Witmer, and C. A. Schuh, *Appl. Phys. Lett.* **92**, 171911 (2008).
- [76] M. Kardar and Y. C. Zhang, *Phys. Rev. Lett.* **58**, 2087 (1987).
- [77] T. Baumberger and C. Caroli, *Adv. Phys.* pp. 279–348 (2006).
- [78] J. Zhang, T. Majmudar, A. Tordesillas, and R. Behringer, *Granular Matter* **12**, 159 (2010).
- [79] J. Török, S. Krishnamurthy, J. Kertész, and S. Roux, *Phys. Rev. Lett.* **84**, 3851 (2000).
- [80] M. Talamali, V. Petäjä, S. Roux, and D. Vandembroucq, unpublished (2011).